NIH Public Access
Author Manuscript
Cancer Discov. Author manuscript; available in PMC 2014 November 01.

Published in final edited form as:
Cancer Discov. 2013 November ; 3(11): . doi:10.1158/2159-8290.CD-13-0397.

Autophagy Sustains Mitochondrial Glutamine Metabolism and Growth of BRAF^{V600E}–Driven Lung Tumors

Anne M. Strohecker[1,2], **Jessie Yanxiang Guo**[1,2], **Gizem Karsli-Uzunbas**[1,2], **Sandy M. Price**[1,2], **Guanghua Jim Chen**[1,2], **Robin Mathew**[1,2], **Martin McMahon**[3], and **Eileen White**[1,2,4]

[1]Cancer Institute of New Jersey, 195 Little Albany Street, New Brunswick NJ 08903

[2]Department of Molecular Biology and Biochemistry Rutgers University, 604 Allison Road, Piscataway, NJ 08854

[3]Helen Diller Family Comprehensive Cancer Center & Department of Cellular & Molecular Pharmacology, 1450 Third Street, MC 0128 PO Box 589001, University of California, San Francisco, CA 94158

Abstract

Autophagic elimination of defective mitochondria suppresses oxidative stress and preserves mitochondrial function. Here, the essential autophagy gene *Atg7* was deleted in a mouse model of BRAF^{V600E}-induced lung cancer in the presence or absence of the tumor suppressor TRP53. *Atg7* deletion initially induced oxidative stress and accelerated tumor cell proliferation in a manner indistinguishable from *Nrf2* ablation. Compound deletion of *Atg7* and *Nrf2* had no additive effect suggesting that both genes modulate tumorigenesis by regulating oxidative stress, revealing a potential mechanism of autophagy-mediated tumor suppression. At later stages of tumorigenesis, *Atg7* deficiency resulted in an accumulation of defective mitochondria, proliferative defects, reduced tumor burden, conversion of adenomas and adenocarcinomas to oncocytomas, and increased mouse lifespan. Autophagy-defective tumor-derived cell lines were impaired in their ability to respire, survive starvation and were glutamine-dependent, suggesting that autophagy-supplied substrates from protein degradation sustains BRAF^{V600E}-tumor growth and metabolism.

Keywords

autophagy; BRAF; lung cancer; mitochondria; metabolism; NRF2

Introduction

Autophagy is a catabolic process activated by metabolic stress whereby cellular proteins and organelles are engulfed and targeted to lysosomes for degradation. This process sustains metabolism by recycling intracellular components for use in macromolecular synthesis and prevents the accumulation of damaged proteins and organelles that can be toxic. The role of autophagy in cancer is complex and still poorly understood (1). Mice with allelic loss of the essential autophagy gene *Beclin1* are tumor prone and mosaic or liver-specific deletion of *Atg5* or *Atg7* produces benign hepatomas, suggesting a role for autophagy in tumor suppression (2–4). However, autophagy localizes to metabolically stressed, hypoxic regions of solid tumors where it enables tumor cell survival (5–7). Indeed, KRAS^{G12D}-driven

[4]Corresponding author: Dr. Eileen White, The Cancer Institute of New Jersey, 195 Little Albany Street, New Brunswick, NJ 08903, eileenpwhite@gmail.com, VOICE: (732) 235-5329, FAX (732) 235-5795.

The authors disclose no potential conflicts of interest

NIH-PA Author Manuscript
NIH-PA Author Manuscript
NIH-PA Author Manuscript

NIH-PA Author Manuscript

NIH-PA Author Manuscript

NIH-PA Author Manuscript

tumors upregulate autophagy which is required for maintenance of functional mitochondria, survival during starvation, and tumor growth (8, 9). In the absence of autophagy, defective mitochondria accumulate, triggering a reduction in mitochondrial respiration that is ultimately incompatible with proliferation. This compromises stress tolerance, prompting us to label these tumors “autophagy-addicted” (8–10). Autophagy addiction was recently confirmed in genetically engineered mouse models of $KRAS^{G12D}$–driven non-small-cell lung cancer (NSCLC) where autophagy deletion converted adenomas and adenocarcinomas to oncocytomas, a benign tumor type associated with an accumulation of defective mitochondria (11–14). Thus, the emerging picture is that the role of autophagy in cancer is context-dependent. In some settings autophagy may limit tumorigenesis by preserving protein and organelle quality control (preventing oxidative stress and tissue damage) while in other contexts autophagy promotes metabolism, adaptation to stress and tumor growth. A comprehensive understanding of the role of the pathway in different tissue types as well as the spatial and temporal variations in autophagy-dependence in tumors driven by specific oncogenic events will be required before modulation of autophagy can become an effective therapeutic strategy for cancer (15–17).

Since $KRAS^{G12D}$ driven tumors are exquisitely sensitive to autophagy inhibition, we turned our attention to its downstream effector BRAF. Mutations in *BRAF* are found in many human tumors including melanoma (65%) lung (3%) papillary thyroid (40%) ovarian (4%) and colorectal cancers (18%) (18–20) with the most common alteration being a valine to glutamic acid substitution at residue 600 ($BRAF^{V600E}$) leading to constitutive activation of the kinase and RAS independence. To examine the role of autophagy in $BRAF^{V600E}$–driven lung cancers, mice with Cre-activatible $BRAF^{V600E}$ with and without conditional alleles of the essential autophagy gene *Atg7* were generated, lung tumorigenesis was induced via intra-nasal administration of adenoviral Cre recombinase, and the resulting tumors were followed over time. Additionally, conditional alleles of the tumor suppressor *Trp53* were bred into the *Braf* and *Atg7* compound mutant mice to assess the consequences of *Trp53* loss on the need for autophagy to sustain metabolism and tumorigenesis in the mouse lung.

We report here that autophagy is required for growth of $BRAF^{V600E}$–driven lung tumors and identify the metabolic alterations underlying autophagy addiction. Moreover, we provide direct evidence that the tumor suppressive function of autophagy can be explained by reactive oxygen species (ROS) mitigation early in tumorigenesis. Most importantly, the dominant tumor promoting function of autophagy can be explained by preservation of mitochondrial function and the supply of metabolic substrates that confer stress tolerance likely necessary for sustained tumorigenesis. Thus, autophagy prevents metabolic dysfunction and ensures the health of $BRAF^{V600E}$-driven lung tumors.

Results

Deletion of *Atg7* blocks autophagy in $BRAF^{V600E}$–driven lung cancer

To examine the role of autophagy in tumor establishment and progression, mice homozygous for a Cre-activatible $Braf^{CA}$ allele (21) were mated to $Atg7^{flox/flox}$ mice (22), generating animals in which intranasal administration of adenoviral Cre recombinase simultaneously enabled expression of the oncogenic $BRAF^{V600E}$ variant while deleting the floxed allele of *Atg7* in the mouse lung. The $BRAF^{V600E}$ model was chosen both for its rapid progression (hyperplasia in 2–4 weeks with discrete adenoma formation by 6–8 weeks) and for the capacity to give rise to a spectrum of malignancies when mated to loss- and gain-of-function tumor models. The $BRAF^{V600E}$ mouse lung tumor model yields benign adenomas unless crossed to mice with deletions of known tumor suppressors *INK4A/ARF* or *TRP53*, at which point the lesions progress to adenocarcinomas (21). Thus, the $BRAF^{V600E}$ mouse lung tumor model enables direct testing of the hypothesis that autophagy

NIH-PA Author Manuscript

NIH-PA Author Manuscript

NIH-PA Author Manuscript

functions as a regulator of lung tumorigenesis with the potential to reveal both promotion and inhibition of tumor growth by autophagy.

In this genetically engineered mouse model of lung cancer, all tumors are initiated by the constitutively active $BRAF^{V600E}$ protein (21). *Atg7* deletion and loss of ATG7 protein expression was confirmed by polymerase chain reaction (PCR) (data not shown) and at early (5 and 7 weeks) and late stages (20 and 30 weeks) of tumorigenesis in the $BRAF^{V600E}$-derived tumors by immunohistochemistry (IHC) (Fig. 1A and Fig. S1). ATG7 deletion was detected in tumor and not normal lung tissues as adenoviral-Cre infects only a small fraction of lung cells, and only those with activated $BRAF^{V600E}$ form tumors and expand the population of *Atg7* wild type or deleted cells. Thus, assessment of autophagy function in normal lung is not addressable in this setting. *Atg7* deletion alone by adenoviral-Cre did not cause tumors (Fig. S2 and (13). All tumors were positive for surfactant protein c, a marker of type II alveolar epithelial cells, confirming tumor initiation in the lung (Fig. 1A). Tumor lysates from $Braf^{V600E/+}; Atg7^{-/-}$ mice failed to convert LC3-I to LC3-II, and accumulated the autophagy substrate p62 (Fig. 1B). Similarly, LC3 puncta were visible in the tumor tissue of $Braf^{V600E/+}; Atg7^{+/+}$ mice while only diffuse cytoplasmic staining was detected in tumor tissues from the $Braf^{V600E/+}; Atg7^{-/-}$ mice (Fig. 1C). Taken together, these data demonstrate that *Atg7* deletion is sufficient to block autophagy in $BRAF^{V600E}$-driven lung tumors.

Autophagy ablation causes robust early tumor establishment in the lung

Next, we conducted time course analyses to assess tumor burden over time in mice bearing $Braf^{V600E/+}$ and either $Atg7^{+/+}$ or $Atg7^{-/-}$ lung tumors. A marked difference in tumor burden was revealed upon examination of the lung histology. At 5 weeks post Cre, *Atg7* deficient $Braf^{V600E/+}$ tumors increased tumor burden by nearly 40% in comparison to $Atg7^{+/+}$ tumors (Fig. 2A–C). This increased early tumorigenesis in the $Braf^{V600E/+}; Atg7^{-/-}$ mice was also observed in micro-CT analysis of the mice at 3 and 5 weeks post Cre (Fig. S3). Thus, *Atg7* deficiency promotes early $BRAF^{V600E}$–driven tumor growth.

Histologically, $Braf^{V600E/+}; Atg7^{+/+}$ tumors displayed mild hyperplasia at 5 weeks, progressed to discrete adenomas at 7 weeks, grew steadily into papillary adenomas at 14 weeks post Cre, and mice died shortly thereafter (Fig. 2D). Allelic loss of *Atg7* in $Braf^{V600E/+}; Atg7^{+/-}$ tumors modestly accelerated growth, illustrated by the presence of small focal adenomas 5 weeks post Cre (data not shown). Importantly, the $Braf^{V600E/+}; Atg7^{-/-}$ tumors exhibited profound adenoma formation as early as 5 weeks post Cre, but by 10 weeks post Cre the tumors displayed signs of blunted growth (Figs. 2A–C and S2).

Autophagy deficiency alters $BRAF^{V600E}$ tumor fate from adenomas to oncocytomas

Examination of the histology revealed that $Braf^{V600E/+}; Atg7^{+/+}$ tumors were adenomas, as expected, whereas $Braf^{V600E/+}; Atg7^{-/-}$ tumors were composed of tumor cells with an enlarged, granular cytoplasm characteristic of oncocytomas (Fig. 2D). Oncocytomas are a rare but predominantly benign tumor type characterized by an accumulation of defective mitochondria (12). Indeed, *Atg7* deficiency similarly altered progression of $KRAS^{G12D}$-driven non-small-cell lung cancers to oncocytomas (13).

Consistent with *Atg7* deficiency altering tumor fate from adenomas to oncocytomas, the autophagy-deficient tumors accumulated significantly more mitochondria than their *Atg7*-expressing counterparts as measured by IHC for Tom20 (Fig. 2E). Electron microscopy (EM) revealed that the abundant mitochondria in the $Braf^{V600E/+}; Atg7^{-/-}$ tumors were swollen and misshapen in contrast to the normal mitochondria observed in the $Braf^{V600E/+}; Atg7^{+/+}$ tumors. Moreover, mitochondria in the $Braf^{V600E/+}; Atg7^{-/-}$ tumors were poorly

NIH-PA Author Manuscript

NIH-PA Author Manuscript

NIH-PA Author Manuscript

functional, measured by markedly decreased enzymatic activity of cytochrome c oxidase, an essential component of the electron transport chain, compared to their *Atg7*-expressing counterparts (Fig. 2E). Reduced expression of Cox IV was observed in tumor lysates from *Atg7*-deficient tumors compared to those expressing *Atg7*, indicating that autophagy ablation results in a functional defect in the mitochondria of these tumors (Fig. 2E, F). Thus, autophagy deficiency is sufficient to alter tumor fate from adenomas to oncocytomas in $BRAF^{V600E}$ lung tumors similarly to those with $KRAS^{G12D}$ mutations.

Atg7 deficiency extends lifespan of mice with $BRAF^{V600E}$–driven lung tumors

Aggressive tumors, such as those driven by oncogenic H or KRAS are dependent on autophagy for survival (8, 9, 13, 15). In keeping with these findings and consistent with the conversion of *Atg7*-deficient tumors to a more benign fate, we observed that complete blockade of autophagy was sufficient to extend and nearly double the survival of mice with $BRAF^{V600E}$ driven lung tumors (p=0.017) (Fig. 2G). Mice with $Braf^{V600E/+}; Atg7^{+/+}$ tumors were the first to succumb, exhibiting a median survival of 16 weeks post Cre. In comparison, $Braf^{V600E/+}; Atg7^{-/-}$ tumor-bearing mice exhibited a median survival of 31 weeks. Tumor-specific allelic loss of *Atg7* or whole body allelic loss of the essential autophagy gene *Beclin1,* which significantly impairs but does not ablate autophagy (23) did not alter survival of mice bearing $BRAF^{V600E}$ lung tumors (Fig. 2G, H), suggesting that complete and not partial ablation of autophagy is necessary to suppress tumor growth and increase mouse survival (23). Of note, the median survival of the $Beclin1^{+/-}$ lung tumor bearing mice (15.1 weeks) was nearly identical to that of mice bearing $Atg7^{+/-}$ tumors (15.8 weeks). Importantly, the accumulation of the autophagy substrate p62 was accelerated in $Braf^{V600E/+}; Atg7^{-/-}$ tumors in comparison to $Braf^{V600E/+}; Beclin1^{+/-}$ tumors, consistent with a more profound autophagy defect induced by *Atg7* deficiency (data not shown).

Increased survival of mice bearing $Atg7^{-/-}$ compared to $Atg7^{+/+}; Braf^{V600E/+}$ tumors was accompanied by reduced tumor cell proliferation assessed by nuclear Ki67staining, and increased p53, p21 and γ-H2AX levels at 14 weeks post Cre administration (Figs. 2I, S4, S5). Comparable numbers of cells in wild type and *Atg7*-deficient tumors were positive for senescence-associated β-galactosidase (Fig. S6A), eliminating senescence as the mechanism for growth arrest and reduced tumor burden with *Atg7* deficiency at 14 weeks. Similarly, no significant changes in active caspase-3 were detected 14 weeks post Cre administration (Fig. S6B).

p53 induction in *Atg7*-deficient $Braf^{V600E}$ lung tumors limits tumor growth

The induction of p53 and p21 in *Atg7*-deficient tumors led us to question whether the mechanism by which autophagy deficiency suppressed tumor proliferation was through induction of a p53 response. To test this hypothesis, we deleted *Trp53* in *Braf* lung tumors with and without *Atg7* and followed tumorigenesis in the resulting mice. Deletion of *Atg7* in *Trp53*-deficient, $BRAF^{V600E}$ lung tumors caused a loss of ATG7 protein expression (residual ATG7 protein is to due the stromal component of the tumor that is not deleted for *Atg7*), the accumulation of LC3, and the autophagy substrate p62 indicative of autophagy inactivation (Fig. 3A). Ablation of *Trp53* did not alter the increased early tumorigenesis of the *Atg7*-deficient tumors, shown as decreased normal/healthy lung volume in the quantitation of the micro-CT analysis at 3 and 5 weeks (Fig. 3B), or the eventual reduction in tumor burden, shown as increased normal/healthy lung volume at 10 weeks, compared to *Atg7* wild type tumors (Fig. 3C). As observed in mice bearing *Trp53*-intact $BRAF^{V600E}$-activated tumors (Fig. 2I), this phenotype was associated with a proliferative defect shown via reduction in nuclear Ki67 staining (Fig. 3D). Kaplan-Meier analysis demonstrated that autophagy deficiency extended the lifespan of tumor-bearing mice independent of p53 status. However, the kinetics are different; mice with *Trp53*-deficient tumors succumb to

NIH-PA Author Manuscript

NIH-PA Author Manuscript

NIH-PA Author Manuscript

their tumors more rapidly than those with intact *Trp53* (Fig. 3E). Thus, loss of ATG7 causes premature p53 induction in $BRAF^{V600E}$ lung tumors that suppresses proliferation and tumor growth. *Atg7*-deficiency suppresses growth of *Trp53*-deficient tumors in a statistically significant manner (p=0.04), revealing a second, *Trp53* independent, growth suppressive mechanism in response to tumor-specific loss of *Atg7*. However, we note that *Trp53* has a major role in suppressing tumor growth and promoting overall survival of mice bearing *Atg7* deleted tumors.

Consistent with the emergence of oncocytomas upon *Atg7* deletion in the $Trp53^{-/-}$; $Braf^{V600E/+}$ lung tumors, these tumors were characterized by the accumulation of defective mitochondria (indicated by increased staining with the mitochondrial marker Tom20), ultrastructural mitochondrial abnormalities, and loss of enzymatic activity for cytochrome c oxidase (Fig. 3F). The fact that *Trp53* deficiency did not influence the conversion of $BRAF^{V600E}$-driven adenocarcinomas to oncocytomas induced by loss of *Atg7* suggests that autophagy is critical to prevent the accumulation of defective mitochondria and maintain adenocarcinoma fate. Importantly, despite the early growth advantage provided by *Atg7* deficiency, tumor growth was ultimately impaired, indicating that the requirement for autophagy to promote tumorigenesis is dominant. Therefore autophagy inhibition may be an important therapeutic tool to alter lung tumor progression to a more benign fate.

Atg7 deficiency induces Nrf2 accumulation in $Braf^{V600E}$ lung tumors

Having established opposing tumor growth suppressing and promoting roles for autophagy in $BRAF^{V600E}$-driven lung tumors, we turned our attention to identifying the underlying mechanisms. One explanation for the early enhancement of tumor growth upon loss of *Atg7* was that increased ROS generated by abnormal mitochondria was responsible. To test this hypothesis, we first examined the levels of the master regulator of antioxidant defense, NRF2, in $Braf^{V600E/+}$; $Atg7^{+/+}$ and $Braf^{V600E/+}$; $Atg7^{-/-}$ tumors. NRF2 is normally ubiquitinated and degraded via the proteasome through its interaction with KEAP1 (24). Autophagy deficiency results in the accumulation of the autophagy substrate p62, which competes with NRF2 for binding sites on KEAP1. Thus, under autophagy deficient conditions, NRF2 accumulates and translocates to the nucleus where it activates the cellular antioxidant defense program (25–29). Indeed, induction of NRF2 was observed in *Atg7*-deficient tumors both by IHC examining levels of nuclear NRF2 and by Western blotting of tumor lysates (Fig. 4A, B). Induction of nuclear NRF2 correlated with p62 accumulation in *Atg7*-deficient tumors as expected (Fig. 4A). However, it was unclear whether this induction was caused by *Atg7* deletion as a consequence of the accumulation of p62, or rather resulted from increased ROS production due to failure of mitochondrial quality control that also induces NRF2 (26). To resolve this question, we examined the functional consequences of *Nrf2* loss in $BRAF^{V600E}$-driven lung tumorigenesis in the presence or absence of *Atg7*.

Nrf2 deficiency enhances early and impedes late $BRAF^{V600E}$ lung tumor growth

Mice with Cre-activatible $Braf^{V600E}$with and without conditional alleles of *Atg7* were mated to *Nrf2* knockout mice, tumorigenesis was induced in the lung via intra-nasal administration of adenoviral-Cre recombinase, and the resulting tumors were followed over time. Surprisingly, *Nrf2* ablation caused a profound yet comparable increase in early tumor growth independent of autophagy status, indicating that the early tumor growth is driven by loss of anti-oxidant defense (Fig. 4C). Compound deficiency in both *Nrf2* and *Atg7* produced no additional increase in early tumor growth compared to loss of either gene alone (Fig. 4C). Stimulation of early tumorigenesis induced by *Nrf2* deficiency was associated with activation of the DNA damage response (γ-H2AX positivity) consistent with elevated ROS production and oxidative stress (Fig. 4D). Compound loss of both *Nrf2* and *Atg7* failed to produce significant increases in the levels of phosphorylated γ-H2AX compared to loss of

NIH-PA Author Manuscript

NIH-PA Author Manuscript

NIH-PA Author Manuscript

either alone, suggesting that they function in the same pathway (Fig. 4D). These findings are consistent with increased positivity for the ROS-specific DNA adduct 8-oxo-2′-deoxiguanosine (8-oxo-dG) in tumor sections upon loss of either or both *Atg7* and *Nrf2* but not in *Atg7* and *Nrf2* wild type tumors at 17 weeks post Cre administration (Figs. 4D, E).

Deficiency in *Nrf2* phenocopies *Atg7* loss in survival analyses

Despite the marked promotion of early tumorigenesis, loss of *Nrf2* extended survival of mice in a similar manner to what was observed with *Atg7* deletion previously: median survival of *Nrf2* intact mice was 17.4 weeks compared to 21.6 weeks for the *Nrf2* deleted mice (p=0.003) (Fig. 4F and 2G). Critically, there was no further increase in survival when both *Atg7* and *Nrf2* were deleted (p=0.61) indicating that *Nrf2* ablation phenocopies *Atg7* loss and that the two genes are epistatic to one another. Further strengthening this argument is the comparable survival of $Nrf2^{+/+}; Braf^{V600E/+}; Atg7^{-/-}$ (26.4 weeks) and $Nrf2^{-/-}; Braf^{V600E/+}; Atg7^{+/+}$ (21.6 weeks) mice (p= 0.55). Thus, loss of either *Nrf2* or *Atg7* or loss of both genes reduces tumor growth and increases survival as previously reported for *Nrf2* deletion in $BRAF^{V600E}$-induced lung tumors (30). Taken together, this suggests that although oxidative stress through loss of antioxidant defense or defective autophagy, or both, stimulates early tumor growth this early promotion of tumor cell proliferation is not sustained and eventually results in a tumor growth defect.

Loss of *Atg7* impairs mitochondrial metabolism and survival during starvation

We hypothesized that the autophagy-deficient tumors eventually fail to thrive because they evolve into oncocytomas that are metabolically compromised. To test this hypothesis, we generated *Atg7*-wild type and -deficient $Trp53^{-/-}; Braf^{V600E/+}$ tumor-derived cell lines (TDCLs) and directed our efforts toward the identification of the metabolic defects responsible for the blunted tumorigenesis observed in the autophagy-deficient setting. Western blot analysis confirmed deficiency in ATG7 in the $Atg7^{-/-}$ TDCLs but not in those derived from $Atg7^{+/+}$ tumors (Fig. 5A). During starvation in HBSS, the autophagy block in the $Atg7^{-/-}$ TDCLs manifested as a persistent accumulation of LC3-I that was not processed to LC3-II (Fig. 5B), confirming that $Atg7^{-/-}$ TDCLs were autophagy deficient (Fig. 5B).

Deficiency in *Atg7* dramatically impaired both starvation survival and tumor growth in nude mice compared to the *Atg7* wild type counterparts (Fig. 5C, D) recapitulating the findings from the genetically engineered mice (Fig. 2G). Consistent with the mitochondrial defects observed with *Atg7* deficiency in tumors in the genetically engineered mice, the autophagy-deficient TDCLs possessed greater numbers of mitochondria yet had a smaller fraction of functional mitochondria than their wild type counterparts (Fig. 5E). Next, we examined the oxygen consumption rates (OCR) of autophagy-competent and -deficient TDCLs maintained in normal growth media (RPMI) or following short-term starvation with HBSS (4 hours) as a first approximation of their metabolic fitness. Basal and starvation-induced OCR levels of the autophagy-deficient TDCLs were significantly lower than the rates measured with the autophagy-competent TDCLs (Fig. 5F). Importantly, the mitochondrial reserve capacity (OCR post-injection of the uncoupler Trifluorocarbonylcyanide Phenylhydrazon FCCP) of the autophagy-deficient TDCLs was nearly absent following starvation, lending further support to the hypothesis that autophagy supplies metabolites which maintain mitochondrial function (Fig. 5F).

We next identified the metabolic component supplied by autophagy that enabled survival during starvation. Addition of exogenous glutamine or to a lesser extent sodium pyruvate, but not glucose, or the ROS scavenger N-acetyl-cysteine (NAC), was sufficient to rescue survival of the *Atg7*-deficient TDCLs in response to starvation (HBSS) in a clonogenic assay (Figs. 5G and S7). This suggests that autophagy deficiency renders TDCLs glutamine-

NIH-PA Author Manuscript

NIH-PA Author Manuscript

NIH-PA Author Manuscript

dependent. The inability of NAC to protect *Atg7*-deficient TDCLs from starvation-induced death suggests that loss of viability does not result from excess ROS production but rather resulted from metabolic insufficiency (Fig. S7). OCR analysis revealed that the autophagy-deficient TDCLs were capable of utilizing glutamine to turn the tricarboxylic acid (TCA) cycle, resulting in an increased OCR compared to glutamine starved conditions, although they were not as efficient at doing so as their autophagy competent counterparts (Fig. 5H). Taken together this data suggests that the failure of the late stage *Atg7*-deficient tumors to thrive is due both to an impairment of overall mitochondrial function and substrate limitation (particularly glutamine) of the remaining functional mitochondria, which together lead to metabolic crisis that is incompatible with continued tumor growth.

Discussion

The role of autophagy in cancer is complex; it can either suppress or promote tumorigenesis depending on cellular context (1, 15). Whether these differential effects of autophagy are due to the artificiality of the models examined or occur in human cancer, remain to be determined. Factors with the potential to influence the role of autophagy in cancer include tissue type, nature of the driver mutations, the metabolic demands imposed by growth and proliferation, level of inherent metabolic stress as well as the particular metabolic pathways engaged. It is clear that physiologic, genetic, and *in vivo* approaches are needed to resolve these issues.

To begin to address the context-dependent role of autophagy in cancer, we ablated *Atg7* in the Cre-activatible mouse model of $BRAF^{V600E}$-driven lung tumorigenesis that normally results in benign tumors (21). We demonstrated that defective autophagy through loss of *Atg7* and the concomitant loss of mitochondrial quality control that increases oxidative stress, promotes early tumorigenesis, revealing a potential mechanism by which autophagy can limit tumor growth. Persistent mitochondrial dysfunction, however, eventually overshadows this initial tumor growth advantage, resulting in metabolic impairment, reduction in tumor burden, the emergence of oncocytomas, and an increase in the overall mouse survival.

Several important points emerge from these studies. First, *Atg7* deficiency in the context of $BRAF^{V600E}$-driven lung tumorigenesis promotes early tumor growth. This initial stimulation of tumor cell proliferation was associated with increased oxidative stress suggesting that it may be a ROS-mediated event. Similarly, loss of the master regulator of antioxidant defense, *Nrf2,* initially promoted proliferation of $BRAF^{V600E}$-driven lung tumors, and loss of both *Atg7* and *Nrf2* provided no additional growth advantage. This suggests that oxidative stress from loss of either autophagy or antioxidant defense may stimulate early $BRAF^{V600E}$ lung tumor growth and that *Atg7* and *Nrf2* are genetically epistatic.

It is well established that ROS induces genomic damage and mutations that can promote cancer, and that autophagy deficiency increases ROS levels, mutation rates, and genome instability (6, 7). However, these consequences of ROS production are unlikely to be playing a role here since the growth promotion induced by *Atg7* or *Nrf2* loss is temporary. ROS activates oncogenic signaling pathways including HIF, Wnt/β-catenin, Notch, and ERK and it is more likely that these signaling events are responsible for the transient growth stimulation observed in the $BRAF^{V600E}$ lung tumors deficient for *Atg7* or *Nrf2.* It remains to be seen whether the eventual diminution of tumor burden observed with *Atg7* or *Nrf2* loss corresponds to the progressive deterioration of mitochondrial function and loss of ROS production. We propose that autophagy deficiency results in the accumulation of malfunctioning mitochondria giving rise to oxidative stress (as is the case with loss of *Nrf2*-

NIH-PA Author Manuscript

NIH-PA Author Manuscript

NIH-PA Author Manuscript

mediated antioxidant defense) that initially stimulates the growth of $BRAF^{V600E}$-driven lung tumors by activating growth promoting signaling pathways. The potential signaling events activated in this setting remain to be determined, although no difference was observed in the levels of phospho-ERK in *Atg7* wild type and deficient $Braf^{V600E}$ lung tumors (data not shown). Alternatively, insufficient levels of autophagy-supplied substrates, such as glutamine from protein degradation, may impair mitochondrial metabolism, ROS production and metabolic fitness (Fig. 6).

Second, autophagy is required for sustaining the growth of $BRAF^{V600E}$-driven lung tumors and for dictating their fate. Specifically, autophagy ablation shifts tumor progression from adenomas (*Trp53* intact tumors) and adenocarcinomas (*Trp53* null tumors) to oncocytomas. This data suggests that altering tumor fate to benign oncocytomas by inhibiting autophagy could be a novel therapeutic approach to $BRAF^{V600E}$-driven lung cancer and may extend to other tumors driven by MAP kinase signaling. Importantly, deficiency in either of the essential autophagy genes *Atg7* or *Atg5* in RAS-transformed cancer cell lines impairs tumor growth and causes the accumulation of defective mitochondria (8, 9) as seen here for $BRAF^{V600E}$-induced tumors. Thus, the oncocytoma phenotype and defective tumor growth are a consequence of defective autophagy and not related to any autophagy-independent function of *Atg7*. Although *Atg7* deficiency also alters the fate of $KRAS^{G12D}$-driven adenomas and carcinomas to oncocytomas (13), in $BRAF^{V600E}$ lung tumors this occurs more rapidly and confers a greater survival advantage, suggesting that MAP kinase signaling may be a key driver for autophagy-dependence. It will be of great interest to test the role of autophagy in other $BRAF^{V600E}$ driven malignancies. It will also be very important to determine whether acute autophagy ablation is sufficient to convert established tumors to oncocytomas.

Production of oncocytic tumors by autophagy ablation was associated with reduced proliferation indicating that cell cycle inhibition was the main cause of reduced tumor burden. Enhanced p53 induction caused by *Atg7*-deficiency contributed to but was not essential for the proliferative arrest in response to *Atg7* deficiency, revealing both p53-dependent and p53-independent mechanisms by which autophagy promotes tumor cell proliferation as is the case with $KRAS^{G12D}$-driven lung tumors (13). Autophagy deficiency (either ablation or allelic loss) activates the DNA damage response (6, 23). Recently, allelic loss of *Beclin1* was shown to activate a p53-mediated block to mammary tumorigenesis (31). Tumors apparently activate autophagy to suppress the p53 response as part of a tumor-promotion mechanism. These findings are consistent with autophagy being of central importance for maintenance of mitochondrial metabolism in RAS-driven tumors (8–10, 13) and extend the generalizability of the phenomenon to include $BRAF^{V600E}$-driven lung tumors and possibly those driven by other oncogenic events (32).

Third, we identify a potential mechanism to explain the eventual growth defect in *Atg7*-deficient $BRAF^{V600E}$-driven lung tumors. Autophagy was originally identified in yeast as a pathway required for survival to nitrogen starvation (33). Mammals also require autophagy to survive starvation (34) as is the case with many cancer cells (1). Autophagy degrades intracellular components to recycle them in metabolic and biosynthetic pathways in times of deprivation (16). Indeed, autophagy deficient $BRAF^{V600E}$ TDCLs were impaired in tumorigenesis, and failed to survive starvation but were dramatically rescued by glutamine supplementation. Thus, *Atg7* deficiency causes dependency on exogenously supplied glutamine likely due to the absence of internally supplied glutamine recycled from autophagy-mediated protein degradation. Thus, autophagy addiction may just be a means to provide the tumor cells with glutamine. It will be important to determine whether the *Atg7*-deficient tumor cells are metabolically exhausted due to substrate limitation, or due to dysfunctional mitochondria, or both. Moreover, it will be important to determine whether

NIH-PA Author Manuscript

NIH-PA Author Manuscript

NIH-PA Author Manuscript

the metabolic frailty of *Atg7*-deficient TDCLs *in vitro* is the direct cause of defective tumor growth *in vivo*.

Deletion of *Atg7* in *Trp53*-deficient and $KRAS^{G12D}$ activated lung tumors resulted in significant inflammation causing pneumonia, and an accumulation of defective mitochondria and neutral lipids secondary to impaired fatty acid oxidation (13). We did not observe inflammation or lipid accumulation with deletion of *Atg7* in the *Trp53*-deficient, $BRAF^{V600E}$-activated lung tumors or in TDCLs *in vitro;* nor did we see the appearance of lipidic cysts in tumor allografts (Fig. S8 and data not shown) suggesting a fundamental difference in metabolism and mitochondrial utilization distinguishing $KRAS^{G12D}$ and $BRAF^{V600E}$ lung tumors. Indeed, in melanoma, $BRAF^{V600E}$ activates pyruvate dehydrogenase promoting pyruvate utilization in the TCA cycle, which drives oncogene-induced senescence (35). It is also well established in melanoma models that $BRAF^{V600E}$ suppresses mitochondrial biogenesis via regulation of the transcription factor *MITF* and peroxisome proliferator-activated receptor gamma, coactivator 1 alpha (PGC1α (36). Mitochondrial quality control may be critically important for $Braf^{V600E}$ malignancies given the context of an already reduced pool of functioning mitochondria undergoing enhanced respiration due to increased pyruvate utilization. Taken together, this work provides valuable insights into where and how autophagy should be modulated in $BRAF^{V600E}$-driven lung tumors and lends further support to the clinical utility of autophagy inhibition for cancer therapy.

Materials and Methods

Animal husbandry and infection

All experiments were conducted in compliance with IACUC guidelines. $Braf^{CA/CA}$ mice were bred to $Atg7^{flox/flox}$ (provided by Dr. M. Komatsu) or $Beclin1^{+/-}$ (provided by Dr. Z. Yue) to generate $Braf^{CA/+}; Atg7^{+/+}$, $Braf^{CA/+}; Atg7^{-/-}$ and $Braf^{CA/+}; Beclin1^{+/+}$ or $Braf^{CA/+}; Beclin1^{+/-}$ mice. Compound *Braf; Atg7* mice were bred to $Trp53^{lox/flox}$ (Jackson Laboratory) or $Nrf2^{-/-}$ (YW Kan) generating triple mutant mice. For adenoviral Cre infection, mice 6–8 weeks of age were anesthetized with isoflourane, and high titer replication defective adenoviral-Cre (4×10^7 pfu/mouse) (University of Iowa Gene Vector Core) was administered intra-nasally as a calcium precipitate. Mice were monitored until fully recovered from the anesthetic before returning to their housing. For allograft studies of the TDCLs, 10^7 cells were injected bilaterally into the flank of 6 week old nude mice (Taconic). Tumor size was measured every 2 days. Mice were sacrificed at 14d post injection. Tumors were fixed for histology as described below.

Micro-CT analysis

Respiratory gated, low resolution CT images of maximally ventilated mice were obtained using a Siemens Inveon PET/CT and the INVEON Acquisition Workplace software. Using INVEON Research Workplace software, reconstructed data were processed through a gaussian filter and tissue determined to be pulmonary was segmented and its volume calculated. 3D reconstructions of normal lung tissue and transverse sections were generated using Osirix software.

Antibodies

The following antibodies were used for Western blotting or IHC analysis: ATG7 (Sigma, Cat#: A2856), Surfactant C protein (Seven Hills Bioreagents, Cat#: WARAB-SPC), LC-3 (Nano Tools, Cat#: LC3-5F10), p62 (antisera raised against MBP full length p62 (8) or purchased from Enzo Life Sciences PW9860-0100), Ki67 (Abcam., Cat#: ab-15580), p53 (Leica, Product Code: NCL-p53-CM5P), p21 (BD Biosciences, Cat#: 56431), active

NIH-PA Author Manuscript

NIH-PA Author Manuscript

NIH-PA Author Manuscript

caspase-3 (Cell Signaling, Cat#: 9661), γ–H2AX (Cell Signaling, Cat#: 2577), Nrf2 (Epitomics, Cat#: 2178-1), Tom20 (Santa Cruz Biotechnology, Cat# sc-11415, Cox-IV (Molecular Probes), 8-oxo-dG (clone 2E2, Trevigen), phospho-Erk (Cell Signaling Cat #4376), NRF2 (Epitomics Cat #2178) Beta actin (Calbiochem Cat #CP01).

Histology

For paraffin sections, lungs were dissected into individual lobes, washed 2x in PBS, then fixed for 4h at RT in 10% buffered formalin solution (Formaldefresh, Fisher Scientific) prior to transfer to 70% EtOH and sectioning. For frozen sections, lung tissue was fixed in 10% formalin, transferred to 15% sucrose for 2 hours before final transfer to 30% sucrose and processing.

Cytochrome C Oxidase Staining

A modified Nadi reaction was conducted as follows. Unfixed frozen sections were stained in Incubating Solution (75mg sucrose in 7.5ml water, 0.2M phosphate buffer pH 7.6, 5mg 3′ diaminobenzidine tetrachloride, 10 mg cytochrome c, 20ug catalase) for 1hr at RT. Catalase (C-10), Cytochrome C (C-2506), and DAB (D-5637) were purchased from Sigma. Slides were washed three times in deionized water, dehydrated in ascending alcohols (50%, 70%, 80%, 95% twice, then 100% twice) prior to mounting and imaging.

Senesence-Associated βGalactosidase Assessment

The β-galactosidase staining was performed per manufacturer's recommendations (Cell Signaling Cat#9860). Briefly, sections were fixed for 10mins in 1X fixative, washed twice with PBS before incubation with β-galactosidase staining buffer overnight at 37C in the absence of CO_2. Samples were briefly counterstained with Eosin to facilitate visualization of tissue.

TDCLs

TDCLs were generated from *p53*$^{-/-}$*; Braf* $^{V600E/+}$ tumors with or without *atg7* at 9 weeks post Cre. TDCLs were cultured in RPMI 1640 medium containing 10% fetal bovine serum (FBS), 1% penicillin/streptomycin, 1 mM sodium pyruvate, and 1 mM sodium bicarbonate at 38.5°C with 8.5% CO_2. Atg7 status in these lines was confirmed by PCR and western blot. TDCLs were further characterized for LC3 and p62 accumulation following starvation prior to usage. No additional authentication was performed.

Bodipy staining

0.6 ×10^6 cells were plated on coverslips in 6 well plates, starved for 24h in HBSS. After starvation, cells were rinsed twice with PBS prior to incubation with Bodipy (1mg/ml) for 15 min and counterstained with DAPI. Slides were rinsed in water and mounted with Prolong Anti-fade Gold and imaged.

Western Blotting

Tumor pieces were snap frozen, then ground in liquid nitrogen with mortar and pestle. Material was lysed in RIPA buffer, and assessed for protein concentration with the Bio-Rad BCA reagent and analyzed via SDS-PAGE gel electrophoresis. For TDCLs, whole cell lysates were prepared as described previously (5).

Mitochondrial Mass and Potential Measurements

Live TDCLs were co-labeled with 25nM Mitotracker-Red CMXRos (Molecular Probes/ Invitrogen) to assess Mitochondrial Membrane Potential (MMP) and 25nM Mitotracker –

NIH-PA Author Manuscript

NIH-PA Author Manuscript

NIH-PA Author Manuscript

Green FM (Molecular Probes/Invitrogen) to measure mitochondrial mass for 30 mins under normal growth conditions. Post labeling, samples were washed twice in growth medium, trypsinized and analyzed by flow cytometry (BD Influx Cell Sorter, BD Biosciences). The mean mitochondrial mass fluorescence is shown. Relative MMP was calculated by dividing the mean MMP fluorescence (red) with the mean of mitochondrial mass fluorescence (green).

Oxygen consumption rate measurement

OCR rates were measured with the Seahorse Biosciences extracellular flux analyzer (XF24) as described previously (8). 0.05×10^6 cells were seeded per well in normal growth media (RPMI with 10% FBS) and allowed to attach 24–30h at 38.5°C and 8.5% CO_2 prior to study. Basal measurements were collected following 4h incubation with either RPMI or HBSS. SRC (maximal respiratory capacity-basal respiration rate) and total reserve capacity were measured by injecting the mitochondrial uncoupler FCCP (1.5μM) and Complex III inhibitor Antimycin (20 μM) from the XF24 ports as indicated. For glutamine utilization experiments, cells were plated as above, incubated with HBSS for 30 minutes, transferred to the Seahorse for analysis where l-glutamine (2mM) was injected via the XF24 port. Measurements were collected pre/post glutamine addition as indicated.

Electron microscopy

Tumors were fixed in 2.5% gluteraldehyde / 4% paraformaldehyde/8 mM calcium chloride in 0.1M cacodylate buffer pH 7.4. Samples were stored at 4C overnight prior to delivery for further processing. They were post-fixed in buffered 1% osmium tetroxide and subsequently dehydrated in a graded series of acetone prior to embedding in epon resin. 90nm thin sections were cut on a Leica EM UC6 ultra-microtome. Sectioned grids were stained with saturated solution of uranyl acetate and lead citrate. Images were captured with an AMT XR41 digital camera at 80 Kv on a JEOL 1200EX transmission electron microscope as described previously (5).

Clonogenic Survival Assays

0.07×10^6 TDCL were seeded in 12 well plates in normal growth media and allowed to attach overnight. The cells were washed twice with PBS prior to incubation with either normal growth media, HBSS, or HBSS supplemented with 1mM sodium pyruvate, 2mM L-glutamine, 4.5g/L glucose, or 4mM NAC as indicated for 3 days. Following starvation, cells were allowed to recover in normal growth media for 4 days before methanol fixation and Giemsa staining. For Figure S7, cells were starved for 3 days and allowed to recover in normal media for 3 days prior to fixation and staining.

Statistics

Statistical analyses were carried out with GraphPad Prism version 5.0. Statistical significance was calculated by 2-way ANOVA with Bonferroni post-test. Significance in the Kaplan-Meier analyses was calculated using the log-rank test. For quantification of tumor burden from IHC slides, specimens were digitized with a Trestle MedScan whole slide scanner. An automated image processing protocol was built on Matlab 2011b. Analysis was performed on whole slide map of each specimen to produce tumor area and total tissue area measurements. Tumor and whole tissue masks were created for each slide. The segmentation masks were used for generation of ratios of tumor burden. For quantitation of IHC a minimum of 200 cells were scored from multiple images for each genotype.

NIH-PA Author Manuscript

NIH-PA Author Manuscript

NIH-PA Author Manuscript

Supplementary Material

Refer to Web version on PubMed Central for supplementary material.

Acknowledgments

This work was supported by grants from the NIH (R37 CA53370, R01 CA130893, RO1 CA163591, RCI CA147961 to EW and CA131261 to MM) and a postdoctoral fellowship from NJCCR to AMS (09-2406-CCR-E0)

We thank M. Komatsu for the conditional *Atg7* mice, Z. Xue for the *Beclin1*$^{+/-}$ mice, and Y. W. Kan for the *Nrf2* knockout mice. We also thank R. Patel for the electron microscopy, N. Campbell for micro-CT, W. Chen for histology quantification, A. Roberts for FACS analysis, CINJ Tissue Analytic Services staff, P. Chin for technical assistance, and members of the White lab for helpful discussions.

Abbreviations

IHC	Immunohistochemistry
ROS	Reactive Oxygen Species
NSCLC	Non Small Cell Lung Cancer
TDCLs	tumor derived cell lines
NAC	N-acetyl-cysteine
Q	glutamine
OCR	Oxygen consumption rate
FCCP	Trifluorocarbonylcyanide Phenylhydrazone
TCA cycle	The Citric Acid Cycle
EM	Electron Microscopy
PCR	Polymerase Chain Reaction

References

1. White E. Deconvoluting the context-dependent role for autophagy in cancer. Nat Rev Cancer. 2012; 12:401–10. [PubMed: 22534666]
2. Qu X, Yu J, Bhagat G, Furuya N, Hibshoosh H, Troxel A, et al. Promotion of tumorigenesis by heterozygous disruption of the beclin 1 autophagy gene. J Clin Invest. 2003; 112:1809–20. [PubMed: 14638851]
3. Takamura A, Komatsu M, Hara T, Sakamoto A, Kishi C, Waguri S, et al. Autophagy-deficient mice develop multiple liver tumors. Genes & development. 2011; 25:795–800. [PubMed: 21498569]
4. Yue Z, Jin S, Yang C, Levine AJ, Heintz N. Beclin 1, an autophagy gene essential for early embryonic development, is a haploinsufficient tumor suppressor. Proc Natl Acad Sci U S A. 2003; 100:15077–82. [PubMed: 14657337]
5. Degenhardt K, Mathew R, Beaudoin B, Bray K, Anderson D, Chen G, et al. Autophagy promotes tumor cell survival and restricts necrosis, inflammation, and tumorigenesis. Cancer cell. 2006; 10:51–64. [PubMed: 16843265]
6. Karantza-Wadsworth V, Patel S, Kravchuk O, Chen G, Mathew R, Jin S, et al. Autophagy mitigates metabolic stress and genome damage in mammary tumorigenesis. Genes & development. 2007; 21:1621–35. [PubMed: 17606641]
7. Mathew R, Kongara S, Beaudoin B, Karp CM, Bray K, Degenhardt K, et al. Autophagy suppresses tumor progression by limiting chromosomal instability. Genes & development. 2007; 21:1367–81. [PubMed: 17510285]

NIH-PA Author Manuscript

NIH-PA Author Manuscript

NIH-PA Author Manuscript

8. Guo JY, Chen HY, Mathew R, Fan J, Strohecker AM, Karsli-Uzunbas G, et al. Activated Ras requires autophagy to maintain oxidative metabolism and tumorigenesis. Genes & development. 2011; 25:460–70. [PubMed: 21317241]
9. Yang S, Wang X, Contino G, Liesa M, Sahin E, Ying H, et al. Pancreatic cancers require autophagy for tumor growth. Genes & development. 2011; 25:717–29. [PubMed: 21406549]
10. Lock R, Roy S, Kenific CM, Su JS, Salas E, Ronen SM, et al. Autophagy facilitates glycolysis during Ras-mediated oncogenic transformation. Molecular biology of the cell. 2011; 22:165–78. [PubMed: 21119005]
11. Gasparre G, Porcelli AM, Lenaz G, Romeo G. Relevance of mitochondrial genetics and metabolism in cancer development. Cold Spring Harb Perspect Biol. 2013:5.
12. Gasparre G, Romeo G, Rugolo M, Porcelli AM. Learning from oncocytic tumors: Why choose inefficient mitochondria? Biochim Biophys Acta. 2011; 1807:633–42. [PubMed: 20732299]
13. Guo JY, Karsli-Uzunbas G, Mathew R, Aisner SC, Kamphorst JJ, Strohecker AM, et al. Autophagy suppresses progression of K-ras-induced lung tumors to oncocytomas and maintains lipid homeostasis. Genes & development. 2013; 27:1447–61. [PubMed: 23824538]
14. Iommarini L, Calvaruso MA, Kurelac I, Gasparre G, Porcelli AM. Complex I impairment in mitochondrial diseases and cancer: parallel roads leading to different outcomes. Int J Biochem Cell Biol. 2013; 45:47–63. [PubMed: 22664328]
15. Amaravadi RK, Lippincott-Schwartz J, Yin XM, Weiss WA, Takebe N, Timmer W, et al. Principles and current strategies for targeting autophagy for cancer treatment. Clin Cancer Res. 2011; 17:654–66. [PubMed: 21325294]
16. Rabinowitz JD, White E. Autophagy and metabolism. Science. 2010; 330:1344–8. [PubMed: 21127245]
17. White E, Karp C, Strohecker AM, Guo Y, Mathew R. Role of autophagy in suppression of inflammation and cancer. Curr Opin Cell Biol. 2010; 22:212–7. [PubMed: 20056400]
18. Davies H, Bignell GR, Cox C, Stephens P, Edkins S, Clegg S, et al. Mutations of the BRAF gene in human cancer. Nature. 2002; 417:949–54. [PubMed: 12068308]
19. Pollock PM, Harper UL, Hansen KS, Yudt LM, Stark M, Robbins CM, et al. High frequency of BRAF mutations in nevi. Nature genetics. 2003; 33:19–20. [PubMed: 12447372]
20. Puxeddu E, Moretti S, Elisei R, Romei C, Pascucci R, Martinelli M, et al. BRAF(V599E) mutation is the leading genetic event in adult sporadic papillary thyroid carcinomas. The Journal of clinical endocrinology and metabolism. 2004; 89:2414–20. [PubMed: 15126572]
21. Dankort D, Filenova E, Collado M, Serrano M, Jones K, McMahon M. A new mouse model to explore the initiation, progression, and therapy of BRAFV600E-induced lung tumors. Genes & development. 2007; 21:379–84. [PubMed: 17299132]
22. Komatsu M, Waguri S, Ueno T, Iwata J, Murata S, Tanida I, et al. Impairment of starvation-induced and constitutive autophagy in Atg7-deficient mice. J Cell Biol. 2005; 169:425–34. [PubMed: 15866887]
23. Mathew R, Karp CM, Beaudoin B, Vuong N, Chen G, Chen HY, et al. Autophagy suppresses tumorigenesis through elimination of p62. Cell. 2009; 137:1062–75. [PubMed: 19524509]
24. Kobayashi A, Kang MI, Okawa H, Ohtsuji M, Zenke Y, Chiba T, et al. Oxidative stress sensor Keap1 functions as an adaptor for Cul3-based E3 ligase to regulate proteasomal degradation of Nrf2. Mol Cell Biol. 2004; 24:7130–9. [PubMed: 15282312]
25. Inami Y, Waguri S, Sakamoto A, Kouno T, Nakada K, Hino O, et al. Persistent activation of Nrf2 through p62 in hepatocellular carcinoma cells. J Cell Biol. 2011; 193:275–84. [PubMed: 21482715]
26. Komatsu M, Kurokawa H, Waguri S, Taguchi K, Kobayashi A, Ichimura Y, et al. The selective autophagy substrate p62 activates the stress responsive transcription factor Nrf2 through inactivation of Keap1. Nature cell biology. 2010; 12:213–23.
27. Kwon J, Han E, Bui CB, Shin W, Lee J, Lee S, et al. Assurance of mitochondrial integrity and mammalian longevity by the p62-Keap1-Nrf2-Nqo1 cascade. EMBO Rep. 2012; 13:150–6. [PubMed: 22222206]

NIH-PA Author Manuscript

NIH-PA Author Manuscript

NIH-PA Author Manuscript

28. Lau A, Wang XJ, Zhao F, Villeneuve NF, Wu T, Jiang T, et al. A noncanonical mechanism of Nrf2 activation by autophagy deficiency: direct interaction between Keap1 and p62. Mol Cell Biol. 2010; 30:3275–85. [PubMed: 20421418]

29. Li QK, Singh A, Biswal S, Askin F, Gabrielson E. KEAP1 gene mutations and NRF2 activation are common in pulmonary papillary adenocarcinoma. J Hum Genet. 2011; 56:230–4. [PubMed: 21248763]

30. DeNicola GM, Karreth FA, Humpton TJ, Gopinathan A, Wei C, Frese K, et al. Oncogene-induced Nrf2 transcription promotes ROS detoxification and tumorigenesis. Nature. 2011; 475:106–9. [PubMed: 21734707]

31. Huo Y, Cai H, Teplova I, Bowman-Colin C, Chen G, Price S, et al. Autophagy opposes p53-mediated tumor barrier to facilitate tumorigenesis in a model of PALB2-associated hereditary breast cancer. Cancer discovery. 2013

32. Wei H, Wei S, Gan B, Peng X, Zou W, Guan JL. Suppression of autophagy by FIP200 deletion inhibits mammary tumorigenesis. Genes & development. 2011; 25:1510–27. [PubMed: 21764854]

33. Tsukada M, Ohsumi Y. Isolation and characterization of autophagy-defective mutants of Saccharomyces cerevisiae. FEBS letters. 1993; 333:169–74. [PubMed: 8224160]

34. Kuma A, Hatano M, Matsui M, Yamamoto A, Nakaya H, Yoshimori T, et al. The role of autophagy during the early neonatal starvation period. Nature. 2004; 432:1032–6. [PubMed: 15525940]

35. Kaplon J, Zheng L, Meissl K, Chaneton B, Selivanov VA, Mackay G, et al. A key role for mitochondrial gatekeeper pyruvate dehydrogenase in oncogene-induced senescence. Nature. 2013; 498:109–12. [PubMed: 23685455]

36. Haq R, Shoag J, Andreu-Perez P, Yokoyama S, Edelman H, Rowe GC, et al. Oncogenic BRAF regulates oxidative metabolism via PGC1alpha and MITF. Cancer cell. 2013; 23:302–15. [PubMed: 23477830]

NIH-PA Author Manuscript

NIH-PA Author Manuscript

NIH-PA Author Manuscript

Statement of Significance

The essential autophagy gene *Atg7* functions to promote $BRAF^{V600E}$-driven lung tumorigenesis by preserving mitochondrial glutamine metabolism. This suggests that inhibiting autophagy is a novel approach to treat $BRAF^{V600E}$-driven cancers.

NIH-PA Author Manuscript
NIH-PA Author Manuscript
NIH-PA Author Manuscript

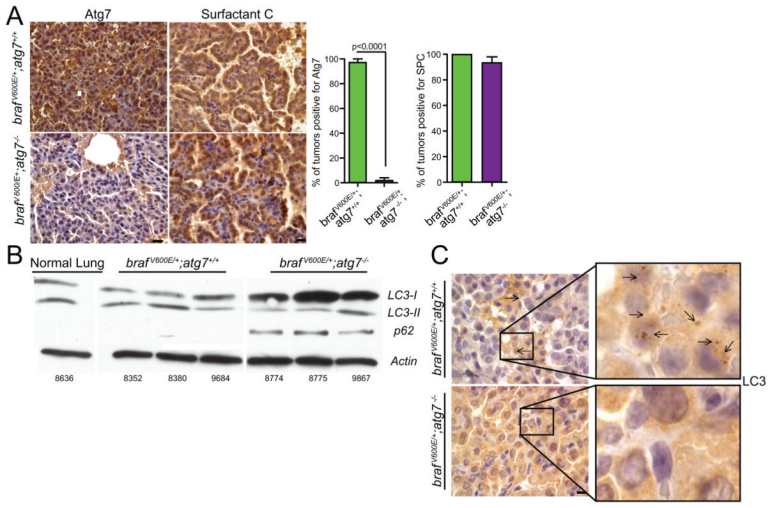

Figure 1. *Atg7* deletion blocks autophagy in a mouse model of *braf*^{V600E}–driven lung tumorigenesis

A. Representative IHC for ATG7 and Surfactant Protein C at 7 (*Braf*$^{V600E/+}$*; Atg7* $^{+/+}$ and *Braf*$^{V600E/+}$*; Atg7*$^{-/-}$) post Cre. Quantification of these data is shown. IHC for ATG7 expression at late time points (20, 30 weeks) is provided in Figure S1. Scale bar= 10μm

B. Western blot analysis of LC3-I to LC3-II conversion, and assessment of p62 accumulation in *Braf*$^{V600E/+}$*; Atg7* $^{+/+}$ and *Braf*$^{V600E/+}$*; Atg7*$^{-/-}$ tumor lysates 10 weeks post Cre. Numbers refer to individual mice. A blank lane was intentionally included between the normal lung and tumor lysates. An additional *Atg7* null tumor lysate was spliced out for aesthetic reasons.

C. Representative IHC staining of LC3 puncta in *Braf*$^{V600E/+}$*; Atg7* $^{+/+}$ and *Braf*$^{V600E/+}$*; Atg7* $^{-/-}$ tumors 8 weeks post infection. Scale bar= 10μm. Arrows denote puncta. Note the absence of puncta and accumulation of diffuse staining in the *Atg7* null tumors.

NIH-PA Author Manuscript
NIH-PA Author Manuscript
NIH-PA Author Manuscript

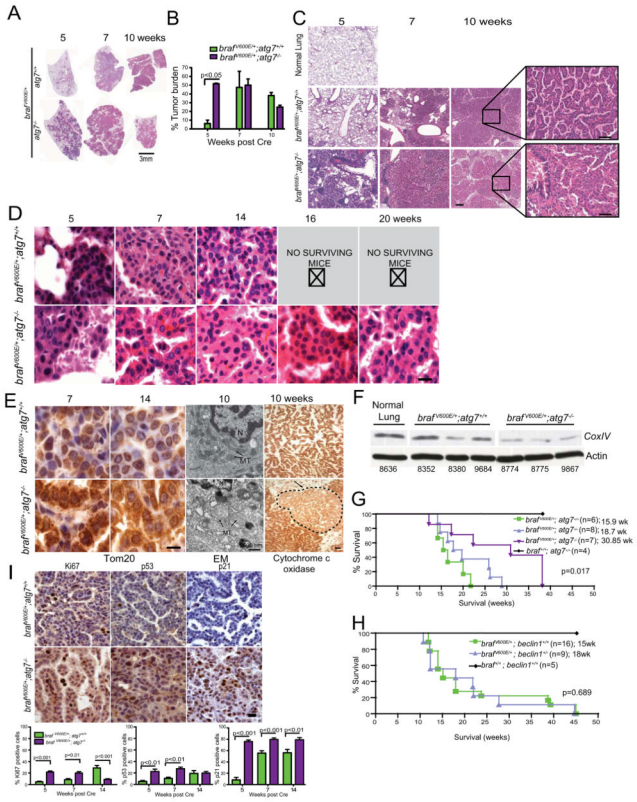

Figure 2. *Atg7* deficiency has distinct consequences for tumor establishment and maintenance in *Braf*^{V600E}–driven lung tumors and is associated with the emergence of oncocytomas and failure of mitochondrial function

A. Representative H&E staining of lung lobes at the indicated times post Cre. Scale bar= 3mm. Scanned H&E slides of the full time course are provided in Figure S2.

B. Quantification of tumor burden (two mice/group, all lobes analyzed) from H&E slides across the indicated time points via Matlab. Error bars indicate SEM. Scanned H&E slides of the full time course are provided in Figure S2.

C. Representative low power images of H&E slides 5, 7, 14 weeks post Cre. Scale bar= 100 μm. Higher magnification images are provided in the inset. Scale bar= 50 μm.

D. Representative high magnification images of H&E staining of tumor for the indicated time course. Note the increasing large cytoplasm in the *Braf* $^{V600E/+}$*; Atg7*$^{-/-}$ tumors indicative of oncocytoma. Scale bar=10 μm

E. *Braf* $^{V600E/+}$*; Atg7*$^{-/-}$ tumors have an accumulation of defective mitochondria. Representative images of Tom20 IHC, electron micrographs, and the enzymatic cytochrome c oxidase assay at the indicated time post Cre. For Tom20, Scale bar= 10μm. For EM, N=nucleus MT= mitochondria. Scale bar=500 nm. Arrows point to swollen mitochondria in *Braf* $^{V600E/+}$*; Atg7*$^{-/-}$ tumors. For cytochrome c oxidase, arrows point to tumor regions, indicated by dashed line, with defective mitochondria in the *Braf* $^{V600E/+}$*; Atg7*$^{-/-}$ tumors. Scale bar =100 μm.

F. Western blot of Cox-IV in tumor lysates of *Braf* $^{V600E/+}$*; Atg7*$^{+/+}$ and *Braf* $^{V600E/+}$*; Atg7*$^{-/-}$ mice 10 weeks post Cre. Numbers refer to individual mice. A blank lane was intentionally included between the normal lung and tumor lysates. An additional *Atg7* null tumor lysate was spliced out for aesthetic reasons.

G. Kaplan Meier analysis of overall survival of *Braf* $^{V600E/+}$*; Atg7*$^{+/+}$ and *Braf* $^{V600E/+}$*; Atg7*$^{-/-}$ mice post Cre. Numbers of animals per group and median survival are indicated.

NIH-PA Author Manuscript

NIH-PA Author Manuscript

NIH-PA Author Manuscript

H. Kaplan Meier analysis of overall survival of *Braf* $^{V600E/+;}$ *Beclin1* $^{+/+}$ and *Braf* $^{V600E/+;}$ *Beclin1* $^{+/-}$ mice post Cre. Numbers of animals per group and median survival are indicated. I. Representative IHC of Ki67, p53 and p21 from *Braf* $^{V600E/+;}$ *Atg7* $^{+/+}$ and *Braf* $^{V600E/+;}$ *Atg7* $^{-/-}$ mice 14 weeks post Cre. Scale bar=10 μm. Quantification of IHC at 5, 7, 14 weeks post Cre is shown below. Images for entire time course are provided in Figure S4.

NIH-PA Author Manuscript
NIH-PA Author Manuscript
NIH-PA Author Manuscript

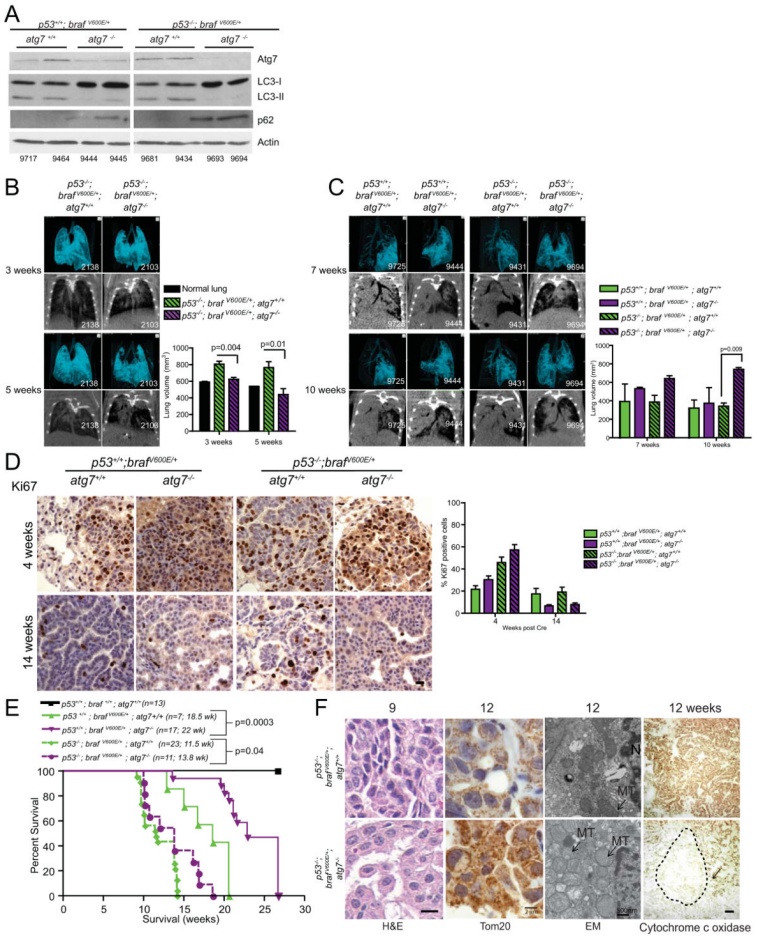

Figure 3. Loss of p53 does not ablate the increased early tumorigenesis or life span extension of mice carrying *Braf* $^{V600E/+}$; *Atg7* $^{-/-}$ tumors

A. Western blot analysis of ATG7 expression, LC3-I to LC3-II conversion, and accumulation of p62 in tumor lysates from *Trp53*$^{+/+}$; *Braf*$^{V600E/+}$; *Atg7*$^{+/+}$, *Trp53*$^{+/+}$; *Braf*$^{V600E/+}$; *Atg7*$^{-/-}$ and *Trp53*$^{-/-}$; *Braf*$^{V600E/+}$; *Atg7*$^{+/+}$, *Trp53*$^{-/-}$; *Braf*$^{V600E/+}$; *Atg7*$^{-/-}$ 14 weeks post Cre. Numbers refer to individual mice.

B. Representative micro-CT images and 3D reconstructions of *Trp53*$^{-/-}$; *Braf*$^{V600E/+}$; *Atg7*$^{+/+}$ and *Trp53*$^{-/-}$; *Braf*$^{V600E/+}$; *Atg7*$^{-/-}$ tumors at 3 and 5 weeks post Cre demonstrating increased tumor in the *Trp53*$^{-/-}$; *Braf*$^{V600E/+}$; *Atg7*$^{-/-}$ mice at early time points. Numbers refer to individual mice. Quantification of normal lung volume is shown at right.

C. Representative micro-CT images and 3D reconstructions of *Trp53*$^{+/+}$; *Braf*$^{V600E/+}$; *Atg7*$^{+/+}$, *Trp53*$^{+/+}$; *Braf*$^{V600E/+}$; *Atg7*$^{-/-}$ and *Trp53*$^{-/-}$; *Braf*$^{V600E/+}$; *Atg7*$^{+/+}$, *Trp53*$^{-/-}$; *Braf*$^{V600E/+}$; *Atg7*$^{-/-}$ tumors at 7 and 10 weeks post Cre demonstrating reduced tumor in the *Trp53*$^{-/-}$; *Braf*$^{V600E/+}$; *Atg7*$^{-/-}$ mice at late time points. Numbers refer to individual mice. Quantification of normal lung volume is shown at right.

D. Representative images of Ki67 staining of *Trp53*$^{+/+}$; *Braf*$^{V600E/+}$; *Atg7*$^{+/+}$, *Trp53*$^{+/+}$; *Braf*$^{V600E/+}$; *Atg7*$^{-/-}$ and *Trp53*$^{-/-}$; *Braf*$^{V600E/+}$; *Atg7*$^{+/+}$, *Trp53*$^{-/-}$; *Braf*$^{V600E/+}$; *Atg7*$^{-/-}$ tumors at 4 and 14 weeks post Cre. Scale bar= 10 μm Quantification is shown at right.

E. Kaplan Meier analysis of overall survival of *Trp53*$^{+/+}$ *and Trp53*$^{-/-}$; *Braf* $^{V600E/+}$; *Atg7*$^{+/+}$ and *Braf* $^{V600E/+}$; *Atg7*$^{-/-}$ mice post Cre. Numbers of mice per group and median survival are indicated on graph. Note: this study was ended at 22 weeks once the p value was highly significant (p=0.0003).

NIH-PA Author Manuscript

NIH-PA Author Manuscript

NIH-PA Author Manuscript

F. Representative images of histology (H&E), Tom20 IHC, electron micrographs, and the enzymatic cytochrome c oxidase assay at the indicated time post Cre. For H&E, Scale bar=10 μm For Tom20, Scale bar= 2 μm. For EM, N=nucleus MT= mitochondria. Scale bar=500 nm. Arrows point to swollen mitochondria in *Trp53*$^{-/-}$*; Braf*$^{V600E/+}$*; Atg7*$^{-/-}$ tumors. For cytochrome c oxidase, arrows point to tumor regions, indicated by dashed lines, with defective mitochondria in the *Trp53*$^{-/-}$*; Braf*$^{V600E/+}$*; Atg7*$^{-/-}$ tumors. Scale bar =100 μm

NIH-PA Author Manuscript
NIH-PA Author Manuscript
NIH-PA Author Manuscript

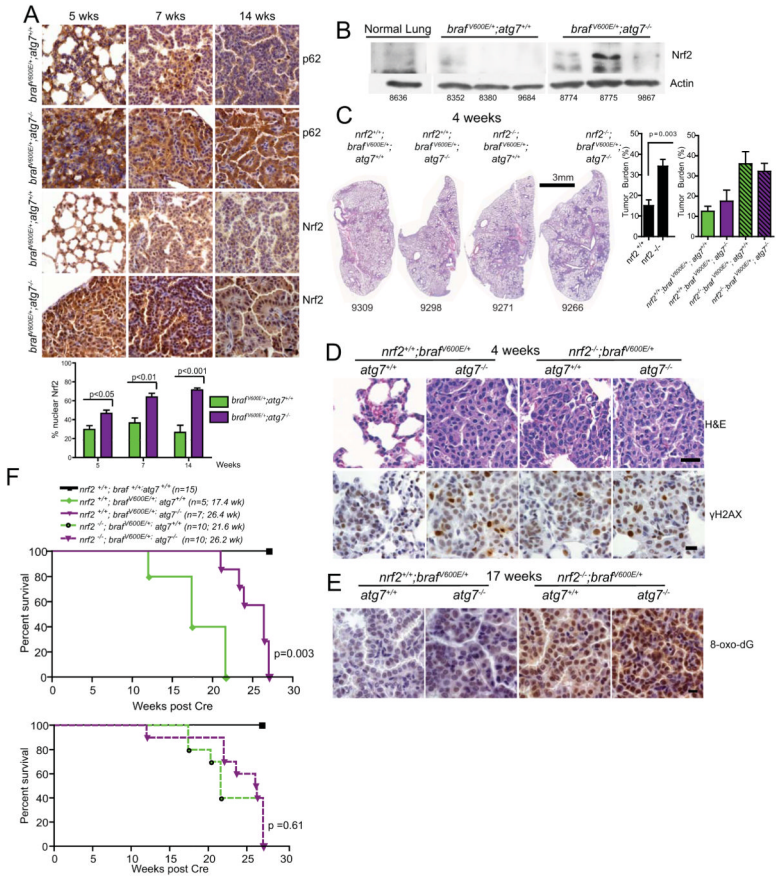

Figure 4. Loss of *Nrf2* phenocopies *Atg7* deletion and is associated with increased lifespan

A. Representative IHC staining for p62 and NRF2 in lung tumors of $Braf^{V600E/+}$; $Atg7^{+/+}$ and $Braf^{V600E/+}$; $Atg7^{-/-}$ mice at the indicated time post Cre. Scale bar=10 μm. Quantification is shown below. Error bars are SEM.

B. Western blot analysis of NRF2 accumulation in lysates of tumors harvested from $Braf^{V600E/+}$; $Atg7^{+/+}$ and $Braf^{V600E/+}$; $Atg7^{-/-}$ mice 10 weeks post Cre. Numbers refer to individual animals. A blank lane was intentionally included between the normal lung and tumor lysates. An additional *Atg7* null tumor lysate was spliced out for aesthetic reasons.

C. H&E staining of single lung lobes showing dramatic increase in size and number of tumors in $Nrf2^{-/-}$ mice independent of autophagy status 4 weeks post Cre. Scale bar= 3 mm. Quantification of tumor burden shown at right. The $Nrf2^{+/+}$ and $Nrf2^{-/-}$ graph is the aggregate of autophagy competent and deficient braf tumors. These data are plotted individually in the next graph. The difference in tumor burden between the $Nrf2^{-/-}$;$Braf^{V600E/+}$; $Atg7^{+/+}$ and $Nrf2^{-/-}$;$Braf^{V600E/+}$; $Atg7^{-/-}$ mice is not statistically significant (p=0.63). The difference in tumor burden between the $Nrf2^{+/+}$;$Braf^{V600E/+}$; $Atg7^{+/+}$ and $Nrf2^{+/+}$;$Braf^{V600E/+}$; $Atg7^{-/-}$ mice is not statistically significant in this experiment (p=0.49). Please refer to similar experiments in Figs. 2A–C, S3, and 3B.

D. Representative images of H&E and IHC analysis of γ-H2AX 4 weeks post Cre. Scale bar=10μm

E. Representative images of IHC for 8-oxo-dG 17 weeks post Cre. Scale bar= 10μm

F. Kaplan Meier analysis of overall survival of the *Nrf2; Braf; Atg7* compound mutant mice. The number of mice per group and median survival are indicated. Note that the increased survival between the $Nrf2^{-/-}$;$Braf^{V600E/+}$; $Atg7^{+/+}$ and $Nrf2^{+/+}$;$Braf^{V600E/+}$; $Atg7^{+/+}$ mice just misses statistical significance (p= 0.06).

NIH-PA Author Manuscript
NIH-PA Author Manuscript
NIH-PA Author Manuscript

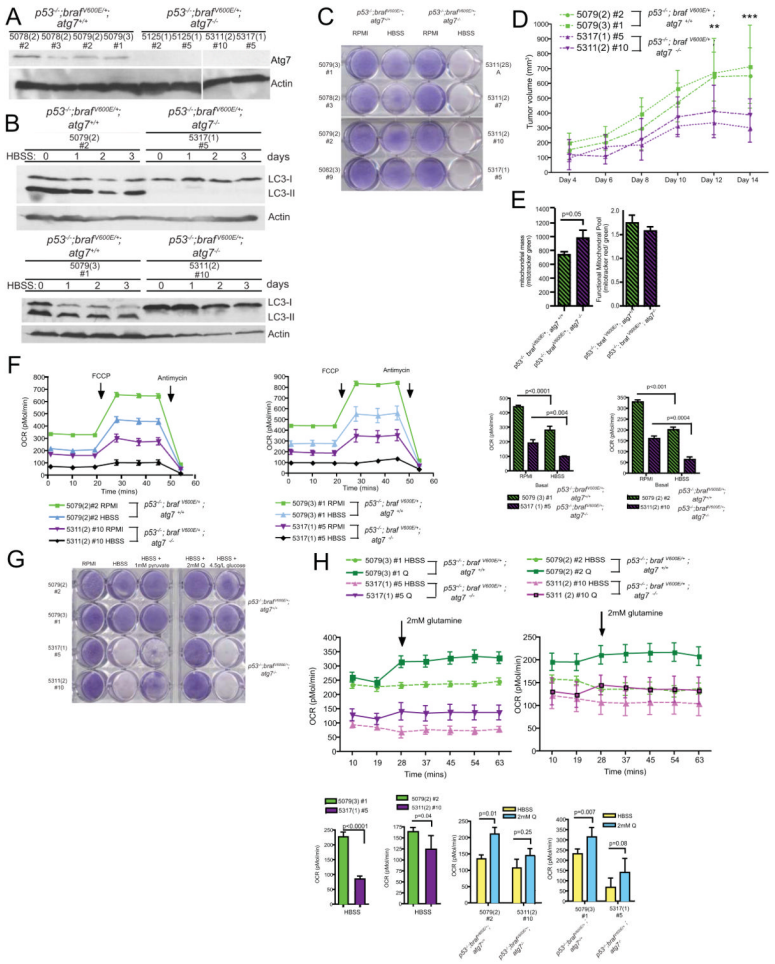

Figure 5. Loss of Atg7 impairs mitochondrial metabolism and survival during starvation

A. Western blot analysis of ATG7 expression in TDCLs isolated 9 weeks post Cre from *Trp53*$^{-/-}$; *Braf*$^{V600E/+}$; *Atg7* $^{+/+}$ or *Trp53*$^{-/-}$; *Braf*$^{V600E/+}$; *Atg7* $^{-/-}$ mice. Numbers refer to individual clones. An additional *Atg7* null tumor lysate was spliced out for aesthetic reasons.

B. Western blot analysis of conversion of LC3-I to LC3-II during a 3 day HBSS starvation time course. Numbers refer to individual clones. Two pairs of ATG7 wild type and ATG7 null derived TDCLs are shown.

C. Clonogenic assay of autophagy-competent or -deficient TDCLs following 3 days of HBSS starvation and 4 day recovery in normal growth media.

D. Allograft growth of *Trp53*$^{-/-}$; *Braf*$^{V600E/+}$; *Atg7* $^{-/-}$ and *Trp53*$^{-/-}$; *Braf*$^{V600E/+}$; *Atg7* $^{+/+}$ TDCLs. n=8 tumors from each genotype were monitored.

E. FACS analysis of Total Mitochrondrial Mass and Relative Mitochondrial Membrane Potential (MMP) of TDCLs.

F. Seahorse measurement of basal and reserve oxygen consumption rates (OCR) of autophagy-competent and -deficient TDCLs under normal growth conditions or following 4hr HBSS starvation.

G. Clonogenic survival of TDCLs incubated with RPMI, HBSS, or HBSS supplemented with exogenous glutamine (2mM), sodium pyruvate (1mM) or glucose (4.5g/L) during 3 day HBSS starvation and 4 day recovery in normal growth media.

H. Seahorse measurement of OCR in the TDCLs incubated with HBSS before and after the addition of 2mM glutamine (Q). Injection timing is indicated by arrow.

NIH-PA Author Manuscript

NIH-PA Author Manuscript

NIH-PA Author Manuscript

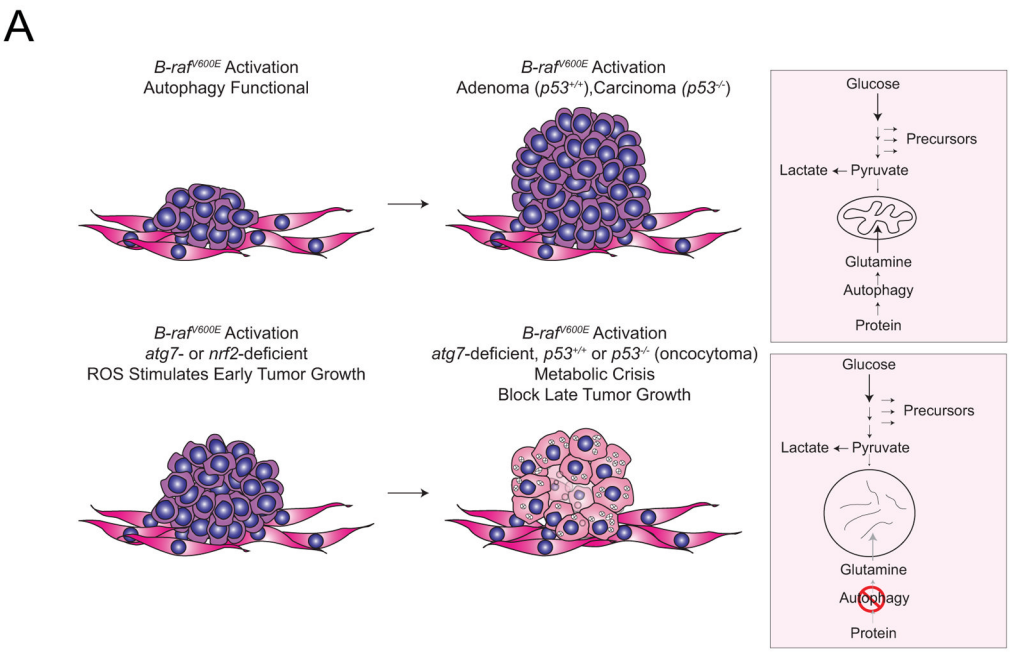

Figure 6. Role of *Atg7* in the growth of *Braf*^{V600E}-driven lung tumors
See text for details.